J Solid State Electrochem (2001) 5: 419–430
DOI 10.1007/s100080000155

ORIGINAL PAPER

M. Noel · N. Suryanarayanan · V. Suryanarayanan

Electrochemical behaviour of Ni, Cu, Ag, Pt and glassy carbon electrodes in triethylamine-tris(hydrogen fluoride) medium

Received: 2 February 2000 / Accepted: 17 June 2000 / Published online: 23 May 2001

Abstract Voltammetric responses of Ni, Cu, Ag, Pt and glassy carbon (GC) electrodes in triethylamine-tris(hydrogen fluoride) medium in the anodic as well cathodic potential region were investigated. AAS as well as SEM measurements were also made to ascertain the dissolution rate and surface transformation due to fluoride film formation on the electrode surfaces. On Ni, bulk NiF_2 film growth occurs only around 4.0 V following a thin NiF_2 monolayer formation around 0 V. The NiF_2 film shows very little solubility in the medium. Monolayer and bulk CuF_2 phases are formed quite close to each other on Cu during anodic polarization. The anodically formed CuF_2 dissolves to the extent of 12% in this medium. AgF formation follows a different mechanism during the first and subsequent anodic sweeps. The effect of MeCN as well as water addition on the solubility and stability of these fluoride films are also reported. Glassy carbon and Pt electrodes are relatively inert in this medium. Anodic voltammetric responses for other reactive species could be observed only on Pt and GC electrodes. On the cathodic side, all the electrodes show inert behaviour. Electrochemical reduction of $PhNO_2$, for example, could be observed on all the electrodes.

Keywords Triethylamine-tris(hydrogen fluoride) · Nickel dissolution · Copper dissolution · Ag dissolution · Fluoride films · Anodic and cathodic polarization

M. Noel (✉) · V. Suryanarayanan
Central Electrochemical Research Institute,
Karaikudi 630 006, India
E-mail: organic@cscecri.ren.nic.in
Fax: +91-4565-27779

N. Suryanarayanan
Alagappa Chettiar College of Engineering,
Karaikudi 630 006, India

Introduction

A number of electrode materials are being employed in different highly concentrated fluoride media of interest in fluorine electrochemistry. In anhydrous HF (AHF) media, Ni and Pt are among the least corroding materials [1, 2]. Ni has received considerable attention in this medium, because of its use as the only anode material in electrochemical perfluorination reactions [3]. A thin passive NiF_2 layer is formed below 1.0 V [4]. Further anodic current noticed beyond 3.0 V [4, 5, 6] has been attributed to additional NiF_2 film growth formation of higher valent nickel fluorides [7], fluorine radical generation [6] and fluorine evolution [5]. Voltammetric studies in the presence of organic compounds suggest electrochemical perfluorination through organic adsorption [8]. During anodic polarization of Cu in AHF, a thick CuF_2 film is formed and the Cu/CuF_2 system functions as a well-defined reference electrode in this medium [9]. Below the F_2 evolution region, Pt [10, 11, 12] and glassy carbon (GC) electrodes [10, 11] serve as stable inert electrodes for voltammetric studies of organic reactions.

Even in AHF, Ni undergoes considerable anodic dissolution in the presence of alkali metal fluorides. Hence in cryolite [13], as well as KF.2HF melts [14], carbon electrodes are mainly employed. Under normal conditions, a thin C-F layer formed on carbon electrodes in a KF.2HF melt does not inhibit electron transfer to any significant extent [14, 15, 16]. Highly passivating anode effects can be eliminated by addition of alkali metal fluoride on the electrode surface or in the electrolyte [15, 17, 18]. Cu undergoes quite reversible redox reactions while Ni shows a passivation phenomenon in this medium as well [19, 20]. Mg, which finds application as bas-bar material in F_2 generators, undergoes considerable dissolution especially in the temperature range 80–90 °C [21].

Ni is once again the electrode of choice for the production of high-purity NF_3 in NH_4F-containing melts.

Tasaka and co-workers [22, 23, 24, 25, 26, 27] have studied the anodic behaviour of Ni in NH_4F-HF as well as in CsF-NH_4F-HF media. Trace level water was found to decrease the corrosion rate of Ni in this medium [25]. The anodic behaviour of Cu has also been studied in this medium [28].

Pyridinium-HF [29, 30] and tetraalkylammonium fluoride-HF [31, 32] have been used in electroorganic synthesis. Pt and carbon electrodes can be employed as inert electrodes in these media over a wide potential range. Triethylamine-tris(hydrogen fluoride) (TEA.3HF) is another highly concentrated fluoride media with good ionic conductivity [33]. The inert behaviour of Pt [34] and the redox behaviour of Ag/AgF [35] have also been studied briefly in this medium. TEA.3HF [36, 37] and TEA.5HF [38] have also been employed in electroorganic synthesis, mainly using Pt electrodes. There is, however, considerable scope for further investigation of different electrode materials in TEA.3HF medium.

The electrochemical behaviour of Ni in aqueous [39] and non-aqueous [40, 41] fluoride media were evaluated in this laboratory. In the present work, the electrochemical behaviour of Ni, Cu, Ag, Pt, and carbon electrodes are compared under identical conditions using electrochemical and surface analytical methods. An attempt is also made to compare the results with those obtained in a number of other concentrated fluoride media cited above.

Experimental

TEA.3HF was prepared by mixing TEA with freshly distilled AHF (TANFAC, India) at the temperature range of a freezing mixture, evaluating the HF content by titration and adjusting the TEA.3HF ratio accordingly [42]. Pt (0.126 cm^2), Cu, Ag, Ni (0.196 cm^2) and GC (0.05 cm^2) rods tight-fitted into Teflon served as the working electrodes. A Pt foil served as the counter electrode. Though neat TEA.3HF and other fluoride media employed in the present work are not aggressive towards glass, a polypropylene undivided cell was used throughout. The choice of reference electrode posed some serious problems. The palladium Pd/H_2 electrode showed instability, especially in TEA.3HF in which Pd dissolution was noticed. Hence, a Pt wire was used as a quasi reference electrode in TEA.3HF. The measurements suggested that the Pt quasi reference potential in TEA.3HF is always close to the Pt/H_2 reference electrode within the limit of $+20$ to $+30$ mV. The reference potential, however, was compared from time to time externally against a saturated calomel electrode (SCE).

MeCN (HPLC) and triply distilled water were used as the additives. Nitrobenzene (AR, Ranbaxy) was used without purification. All the working electrodes were polished to a mirror finish and washed repeatedly with triply distilled water and then with trichloroethylene before use. Since an insoluble fluoride film is formed on Ni, Cu and Ag electrodes during each potential cycle, these electrodes had to be repeatedly cleaned and polished after each CV experiment, in order to obtain reproducible results.

A Wenking potentiostat (model VSG 72) was used for potential control and programming and a Rikadenki (model NP-0363) was used to record the results. SEM was performed with a JEOL (model 30CF) scanning electron microscope. The amount of Ni^{2+} and Cu^{2+} species dissolved in the electrolyte was estimated using atomic absorption spectroscopy (GBC 906AA, Australia). All the experiments were carried out at 303 ± 1 K.

Results and discussion

Anodic behaviour of Ni

Typical cyclic voltammograms obtained during the anodic polarization of Ni in TEA.3HF at different sweep rates are presented in Fig. 1. A small well-defined anodic peak is noticed around 0.0 V. Another well-defined wave is noticed beyond 4.0 V. The first anodic peak current increases with sweep rate v. However, the current in the first peak region was much smaller when compared to the current in the second anodic peak region. Hence these two processes were further investigated separately.

The main anodic peak region

The second or main anodic current appears around 4.0 V, increases and becomes a wave to 8.0 V, beyond which a further sharp rise in current (probably due to fluorine evolution) is noticed. All further studies were thus confined to 8.0 V. Since the current rises with a varying slope from 4.0 to 8.0 V (see Figs. 1 and 2), the peak potential, peak current or the limiting current

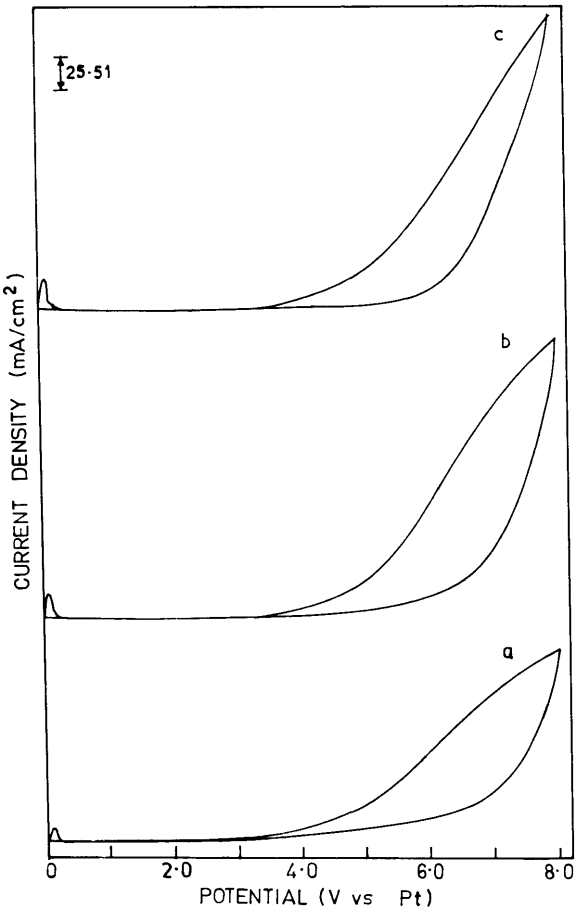

Fig. 1 Cyclic voltammograms (CVs) of Ni in TEA.3HF at different sweep rates (mV s^{-1}): **a** 40, **b** 80, **c** 160

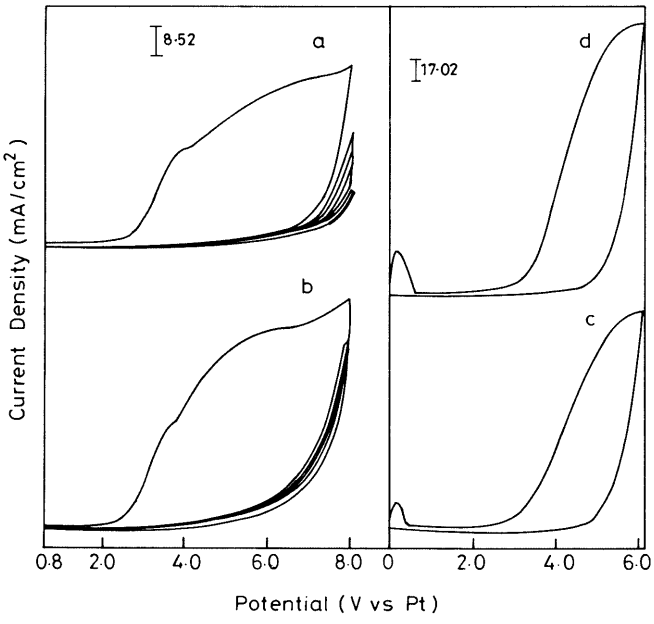

Fig. 2 Multisweep CVs of Ni TEA.3HF containing MeCN of concentration **a** 25%, **b** 50% at 160 mV s^{-1}; CVs of Ni in TEA.3HF containing 10% H_2O in the main anodic potential region at different sweep rates (mV s^{-1}): **c** 80, **d** 160

Table 1 Voltammetric features of Ni in TEA.3HF containing various concentrations of MeCN and H_2O in the main anodic peak region at different sweep rates

Conc. of MeCN (% v/v)	Sweep rate (mV s^{-1})	E_i (V)	Q (C cm^{-2})
0	40	4.0	4.15
	320	4.0	0.76
10	40	3.0	3.43
	320	3.0	0.74
25	40	2.2	2.55
	320	2.3	1.09
37.5	40	2.2	3.24
	320	2.3	1.26
50	40	2.2	4.72
	320	2.3	1.07
75	40	2.5	4.82
	320	2.6	1.74
20% MeCN + 10%H_2O	40	2.4	2.83
	320	2.5	0.44

could not be accurately measured. Hence the initiation potential (E_i) for the process and the anodic charge involved in the potential window from 0 to 8.0 V at different sweep rates are summarized in Table 1. The main anodic peak current does not increase significantly with sweep rate and hence the anodic charge Q_a decreases with increasing v (Table 1). In the reverse sweep, no reduction peak corresponding to the anodic peak was noticed. In multi-sweep cyclic voltammograms, no further anodic current was noticed up to 6.0 V, both in neat TEA.3HF and TEA.3HF containing other additives (Fig. 2).

The effects of two additives, namely acetonitrile, which can influence the solubility of the NiF_2 film formed, and water, which can influence the solubility as well as hydrolysis of NiF_2 to form a passive layer, were examined. In the main peak region, the effect of the additive was significant when the additive content was 10% and above. Typical multi-sweep cyclic voltammograms of Ni in TEA.3HF containing 25% and 50% (v/v) MeCN at a sweep rate of 160 mV s^{-1} are presented in Fig. 2a and b, respectively. The initiation potential (E_i) for anodic dissolution decreases with increasing acetonitrile content (Table 1). However, the anodic dissolution charge decreases with acetonitrile content up to 25% acetonitrile addition. Higher acetonitrile content once again increases the anodic dissolution charge.

The effect of water on the anodic dissolution of Ni was quite similar. Typical cyclic voltammograms of Ni in TEA.3HF containing 10% water are shown in Fig. 2c and d. The E_i values for the main peak are slightly lower than 3.0 V in this medium (Fig. 2c and d and Table 1). The anodic dissolution charge is also slightly lower in TEA.3HF containing 10% water when compared to the same concentration of acetonitrile.

The main anodic peak observed in TEA.3HF is obviously due to the formation of NiF_2 film. Formation of similar, highly insoluble NiF_2 film has been reported in liquid HF media [1, 2, 5, 8]. The film is more soluble in alkali metal fluoride-HF melts [20, 24, 25, 26]. The multi-sweep cyclic voltammograms showing very little anodic current in the second and subsequent sweeps in the present work (Fig. 2) also indicate that the solubility of NiF_2 in TEA.3HF is very low. The rate of film growth is determined by the slow nucleative growth of NiF_2 film and hence the anodic peak current does not increase significantly with sweep rate. The CV responses of Ni presented here are also similar to those studied in detail in acetonitrile-triethylamine-HF media [40, 41].

Despite the similarity in voltammetric responses, the morphology of NiF_2 deposits formed depends significantly on the nature and concentration of the additive employed. Typical SEM images of Ni electrodes in TEA.3HF for 5 min at 5.0 V at different magnifications are shown in Fig. 3a–c. Well-defined NiF_2 crystals on Ni substrates are seen in this figure. The average crystal size is found to be around 5 μm (Fig. 3b). Some crystals up to 30 μm size could also be seen (Fig. 3c). The SEM micrographs obtained after polarization of Ni in the same medium containing 10% (v/v) MeCN at 3.5 V for 5 min (Fig. 3d, e) show significant differences in film structure. The film is quite porous and the crystals are much less distinctly visible (Fig. 3d). Very large sized pits (Fig. 3e) are also noticed in the film.

At slow sweep rates (10 mV s^{-1}), the anodic dissolution charge obtained from CV curves is as high as 15 C cm^{-2}. AAS measurements of the solution after such a polarization indicate very little dissolved Ni^{2+} species in solution (Table 2). If the NiF_2 film is assumed to be compact and uniform, the charge required for a

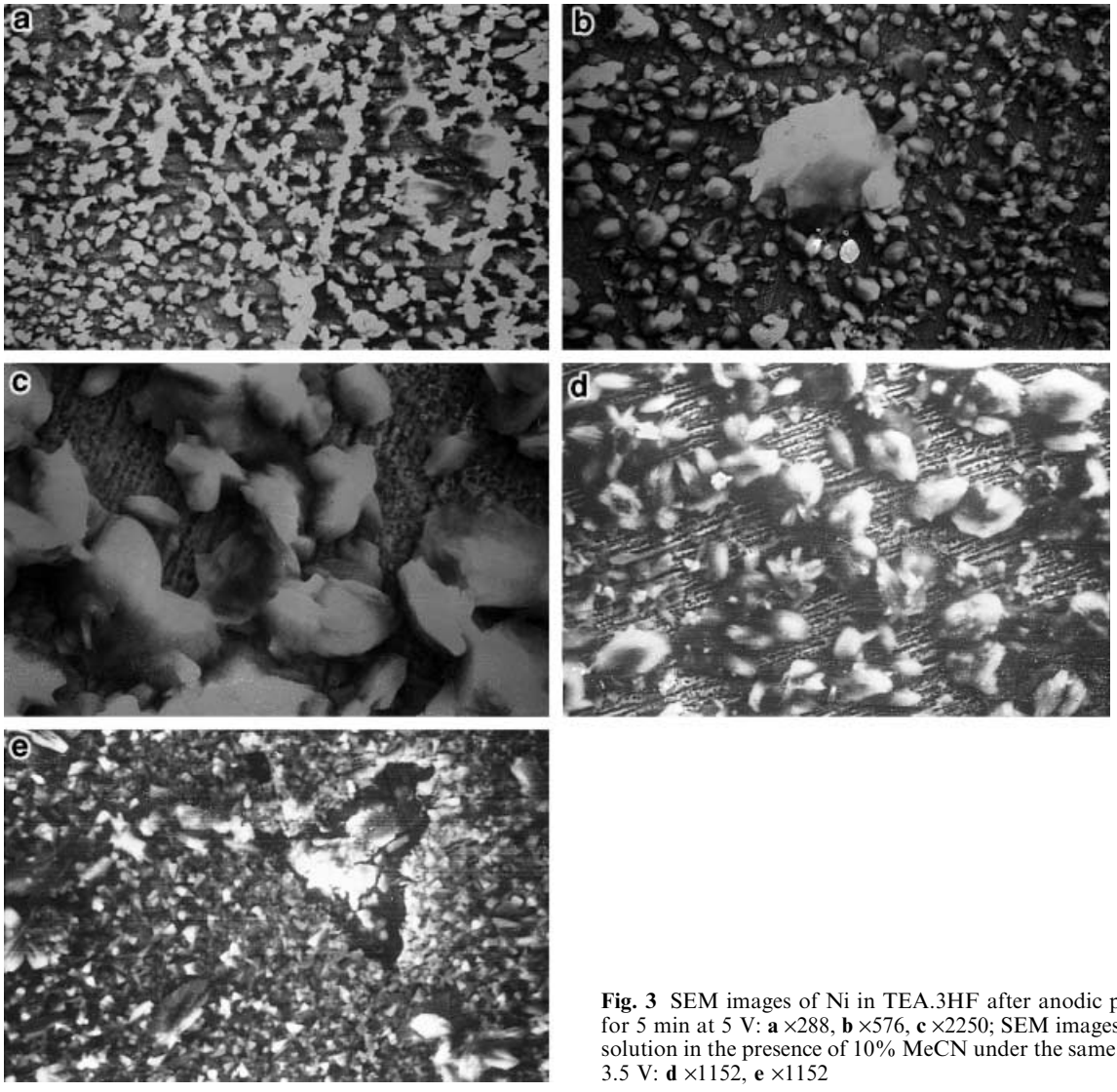

Fig. 3 SEM images of Ni in TEA.3HF after anodic polarization for 5 min at 5 V: **a** ×288, **b** ×576, **c** ×2250; SEM images of the same solution in the presence of 10% MeCN under the same condition at 3.5 V: **d** ×1152, **e** ×1152

monolayer NiF_2 film would be 305 μC cm^{-2}. Even if some allowance is given for surface roughness, the film thickness would be around 100 μm. The formation and stability of such a thick, crystalline layer from TEA.3HF is indeed noteworthy.

Additives seem to influence NiF_2 film dissolution in two ways. A low MeCN concentration, for example 0–25% MeCN, dilutes the fluoride ion content but does not enhance the solubility of NiF_2 in TEA.3HF medium; hence the anodic dissolution charge decreases with MeCN concentration (Table 1). Beyond this concentration, MeCN enhances the solubility of NiF_2 and hence the total anodic dissolution charge increases once again to between 25% and 75% (Table 1).

The first anodic peak region

A small but distinct anodic peak was noticed earlier in liquid HF containing NaF [4] and CsF-NH_4F-HF melts [25, 26, 27]. The anodic process in this region on Ni was studied in some detail in KF-2HF melts [19]. This anodic peak was also observed in TEA.3HF . Despite a lower anodic current, the voltammetric response was highly

Table 2 Metal fluoride formed, dissolved and retained on electrode surfaces

Estimation of fluorides	NiF_2 (moles × 10^{-5})	CuF_2 (moles × 10^{-5})
Total metal fluoride formed (by CV)	8	0.06
Total metal fluoride dissolved (by AAS)	0.002	0.007
Remaining metal fluoride on electrode surface	–	0.05
Percentage of dissolution	>0.1%	12%
Thickness	10 μm	0.07 μm

reproducible, as long as freshly polished electrodes were used for each polarization measurement.

In neat TEA.3HF, at a single voltammetric peak around 0.0 V, the anodic charge involved is around 650 μC cm^{-2} at the slowest sweep rate of 40 mV s^{-1}. The surface charge corresponding to the formation of a monolayer of NiF_2 film is 305 μC cm^{-2}. This suggests either the formation of NiF_2 film with two monolayers or a monolayer film with a Ni surface roughness factor of 2; the latter appears to be more probable.

However, the additive has a substantial effect on the voltammetric behaviour in this region, even at low concentrations. Typical cyclic voltammetric responses of Ni in TEA.3HF containing 2–4% (v/v) MeCN below the 1.0 V anodic limit are presented in Fig. 4. A single well-defined anodic peak around –0.320 V is observed. The anodic peak current increases with concentration as well as sweep rate (Table 3). In the presence of 10% MeCN, for example, an anodic dissolution charge up to 12.2 mC cm^{-2} at 160 mV s^{-1} is found. Thus, although this region corresponds to monolayer formation in the absence of any additive, substantial anodic dissolution can proceed in this potential region itself in the presence of MeCN (Fig. 4).

In the presence of water, two anodic dissolution peaks are noticed in this potential region. Both peaks increase with concentration. While the first peak increases with sweep rate, the second is found to be rather independent of sweep rate (Fig. 5, Table 3). In the presence of 10% (v/v) additives at 40 mV s^{-1}, the total anodic dissolution charge in water (56.6 mC cm^{-2}) is substantially higher than in MeCN (12.2 mC cm^{-2}). The first anodic dissolution peak is probably due to the direct dissolution of Ni and passivation by NiF_2. The second kinetically controlled process is associated with the formation of hydroxides and oxides of Ni. Such passivation effects and formation of reactive conducting oxyfluorides on Ni in the presence of water have been invoked for their electrode activity earlier [25, 27]. In the presence of mixed additives, the dissolution peaks due to individual additives merge and larger dissolution and passivation peaks are noticed (Fig. 6, Table 3).

Overall, during the anodic polarization of Ni in TEA.3HF, the monolayer NiF_2 film formation region and bulk NiF_2 film growth regions are distinctly separated in the potential scale. Both the anodic processes, however, are substantially influenced by solvents such as MeCN and water.

Table 3 Voltammetric features of Ni in TEA.3HF containing various concentrations of MeCN and H_2O in the first anodic peak region at 160 mV s^{-1}

Conc. of MeCN or H_2O (% v/v)	E_{pa} (V)	I_{pa} (mA cm^{-2})	Q (mC cm^{-2})
0	–0.03	1.72	2.00
Conc. of MeCN			
1	–0.32	2.21	3.10
2	–0.32	4.50	4.30
3	–0.32	7.14	6.24
4	–0.34	9.35	8.08
10	–0.39	11.30	12.22
Conc. of H_2O			
1	–0.03	2.98	4.79
2	–0.02	3.83	9.32
3	–0.02	4.26	15.24
4	–0.00	5.96	25.20
10	+0.05	11.46	56.60
10% MeCN + 10% H_2O	–0.18	22.10	62.01

The anodic behaviour of Cu

Typical cyclic voltammograms of Cu in TEA.3HF between –1.2 V to +1.2 V at 160 mV s^{-1} are shown in Fig. 7. Three distinct anodic peaks (a_1, a_2, a_3) are noticed in the forward sweep. The potential reversal beyond peaks a_1, a_2 (Fig. 7a) and a_3 (Fig. 7b) in individual voltammetric measurements show that the oxidized species formed in all these anodic peak potential regions are reduced in the same cathodic peak potential region corresponding to c. The comparison of Q_c/Q_a values for these three anodic limit regions indicate that, in the first anodic potential region, the Q_c/Q_a value is indeed around 0.8 V, suggesting substantially higher cathodic

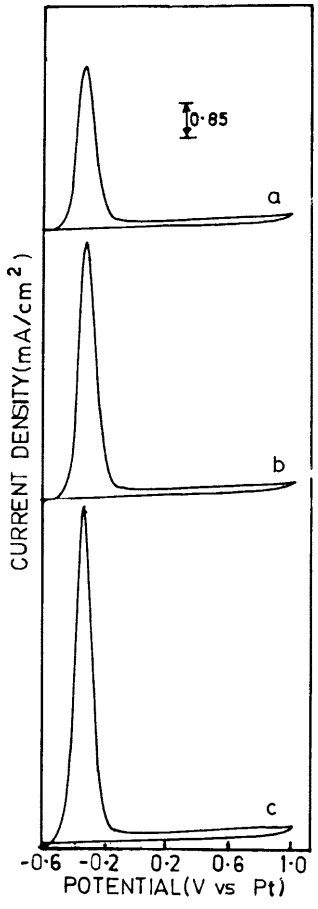

Fig. 4 CVs of Ni TEA.3HF containing MeCN of concentration **a** 2%, **b** 3%, **c** 4% in the first anodic potential region at 160 mV s^{-1}

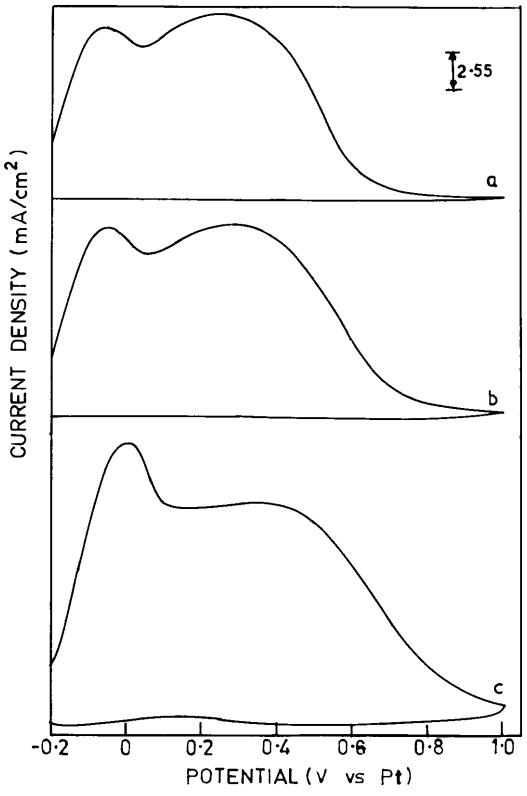

Fig. 5 CVs of Ni TEA.3HF containing 10% of water in the first anodic potential region at different sweep rates (mV s^{-1}): **a** 80, **b** 160, **c** 320

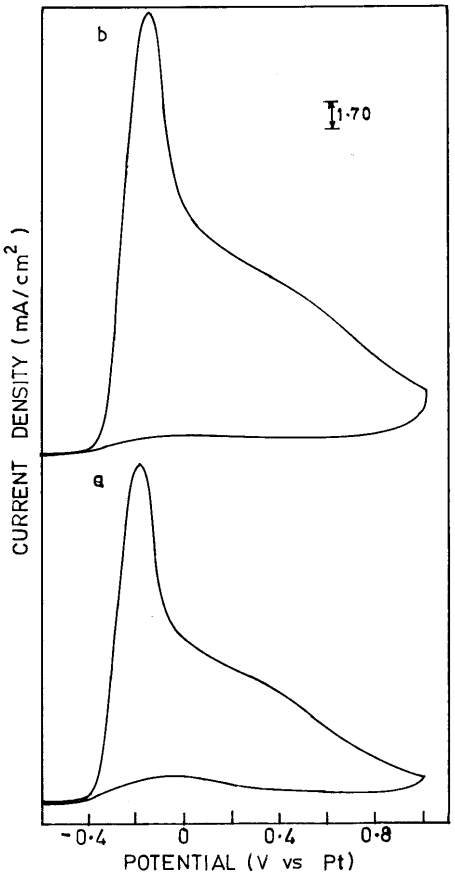

Fig. 6 CVs of Ni in TEA.3HF containing 10% MeCN and water at different sweep rates (mV s^{-1}): **a** 160, **b** 320

charge when compared to the anodic charge involved in the process. The Q_c value of 390 μC cm^{-2} at 160 mV s^{-1} indeed corresponds to the monolayer coverage value (274 μC cm^{-2} for CuF_2 monolayer). However, the Q_a value (1.50 mC cm^{-2}) is substantially higher. It appears that a very thin (4–5 monolayers thick) CuF_2 film is indeed formed in this potential region. If the roughness factor is assumed to be greater than 1, the number of CuF_2 monolayers would be correspondingly lower. Q_a contributes to the anodic formation of CuF_2. In addition, the small residual copper oxide layer likely to be present on the cleaned Cu surface may also be chemically converted into CuF_2 by the following reaction:

$$CuO + 2TEAH^+.H_2F_3^- \rightleftarrows CuF_2 + H_2O + 2TEAH^+.HF_2^- \quad (1)$$

Hence the effective concentration of CuF_2 for reduction at the potential region c_1 is substantially higher.

The other two anodic peaks correspond to bulk film formation. The effect of sweep rate and multi-sweep cycling on these voltammetric peaks are presented in Fig. 8 and Table 4. The multisweep cyclic voltammograms at sweep rates of 80 and 160 mV s^{-1} indicate that the surface redox processes, namely oxidative formation of CuF_2 and reduction of CuF_2 film, can be repeated many times (Fig. 8). The Q_c/Q_a total values obtained at different sweep rates also show that the charge recovery

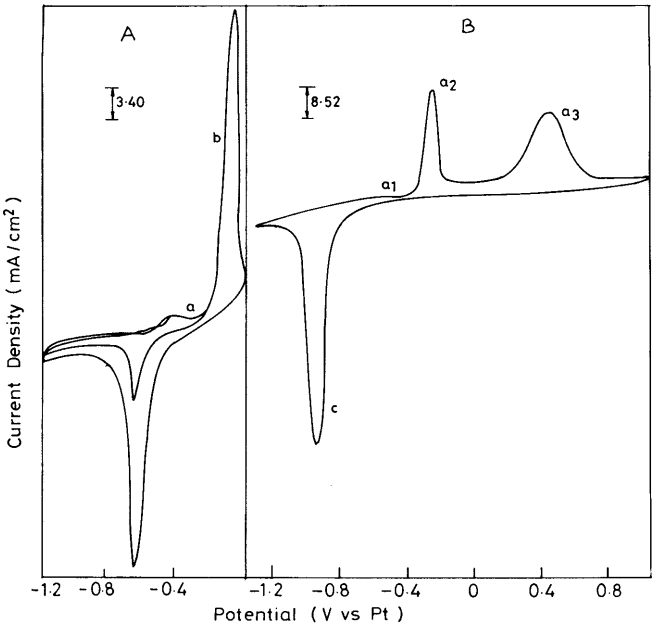

Fig. 7 CVs of Cu in TEA.3HF at different anodic potential limits: **A** –1.2 to 0.0 V; **B** –1.2 to +1.2 V; sweep rate 160 mV s^{-1}

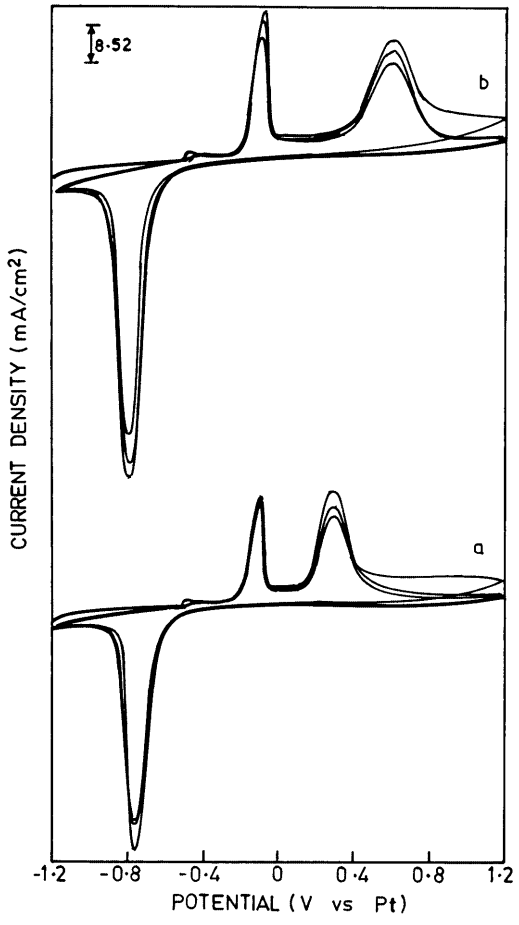

Fig. 8 Multi-sweep CVs of Cu in TEA.3HF at different sweep rates (mV s^{-1}): **a** 80, **b** 160

ratio is greater than 85% (Table 4). AAS measurements also indicate about 12% dissolution of Cu in TEA.3HF after polarization, covering the entire potential region during first cycle (Table 2). These observations suggest that the bulk CuF_2 formed on Cu in TEA.3HF remains intact on the electrode surface and is also stable on potential cycling. Hence this electrode is an ideal one as a reference electrode in TEA.3HF.

The above explanations tacitly made an assumption that the CuF_2 bulk phase is formed in the a_2 as well as a_3 potential region. What would cause the formation of the CuF_2 bulk phase at such widely different potential regions? The effect of sweep rate on the two anodic peaks provides some clues to this issue. The anodic peak a_2 increases with $v^{1/2}$. The E_p value shifts only slightly with sweep rate. The anodic peak current of a_3, however, does not increase significantly with sweep rate. However, the peak potential a_3 shifts substantially to more positive potentials with increasing sweep rate.

The anodic process at a_2 is thus diffusion controlled. This probably occurs through the dissolution and precipitation of Cu to Cu^{2+} and subsequently to CuF_2 film. Taking note of the fact that TEA.3HF in solution is present as $TEAH^+.H_2F_3^-$ and also considering the possibility of HF incorporation in the CuF_2 bulk film during formation, one may write the anodic reaction at a_2 as follows:

$$Cu \rightleftarrows Cu^{2+} + 2e \tag{2}$$

$$Cu^{2+} + mH_2F_3^- \rightleftarrows CuF_2.nHF + (m-n)HF + (m-2)F^- \tag{3}$$

Once this CuF_2 film, formed at potential region a_2, reaches a critical thickness, further growth through this dissolution-precipitation mechanism is impossible. However, at the more positive a_3 potential region, Cu at the Cu/CuF_2 interface may undergo further oxidation for which F^- ions would come from the occluded HF molecules in the CuF_2 film itself:

$$Cu + CuF_2.nHF \rightleftarrows 2CuF_2.(n-2)HF + 2H^+ + 2e \tag{4}$$

Such a slow kinetically controlled oxidation may be the cause of anodic peak a_3. The CuF_2 film essentially is the anodic oxidation product at a_2 as well as a_3; this film becomes reduced at the same cathodic potential region c.

SEM micrographs after anodic polarization of Cu in TEA.3HF by potential cycling are shown in Fig. 9. The Cu oxidation appears to proceed in distinct patches on the Cu surface (Fig. 9a). These patches are also porous on close observation (Fig. 9b). The rough surface morphology does not show significant change during reductive cycles (Fig. 9c, d).

Additives once again exert significant influence on the anodic behaviour of Cu. For example, 4% (v/v) MeCN

Table 4 Voltammetric features of Cu in TEA.3HF containing various concentrations of MeCN and H_2O at 160 mV s^{-1}

Conc. of MeCN or H_2O (% v/v)	E_{pa2} (V)	E_{pa3} (V)	E_{pc} (V)	i_{pa2} (mA cm^{-2})	i_{pa3} (mA cm^{-2})	i_{pc} (mA cm^{-2})	Q_a (mC cm^{-2})	Q_c (mC cm^{-2})	Q_c/Q_a
0	–0.08	0.58	0.80	32.40	23.86	55.38	60.10	40.00	0.66
Conc. of MeCN									
1	–0.06	0.52	–0.80	55.38	31.52	59.60	69.33	58.90	0.84
2	0.10	0.52	0.78	59.64	33.90	61.23	112.0	69.00	0.62
4	0.20	0.52	0.76	85.20	36.64	63.05	169.5	78.17	0.46
Conc. of H_2O									
1	–0.04	0.50	0.72	28.96	25.96	50.38	65.61	59.53	0.90
6	0.01	0.38	0.68	25.12	25.56	30.67	81.90	48.99	0.59
8	0.10	0.30	0.62	23.56	17.04	27.26	90.00	41.48	0.46

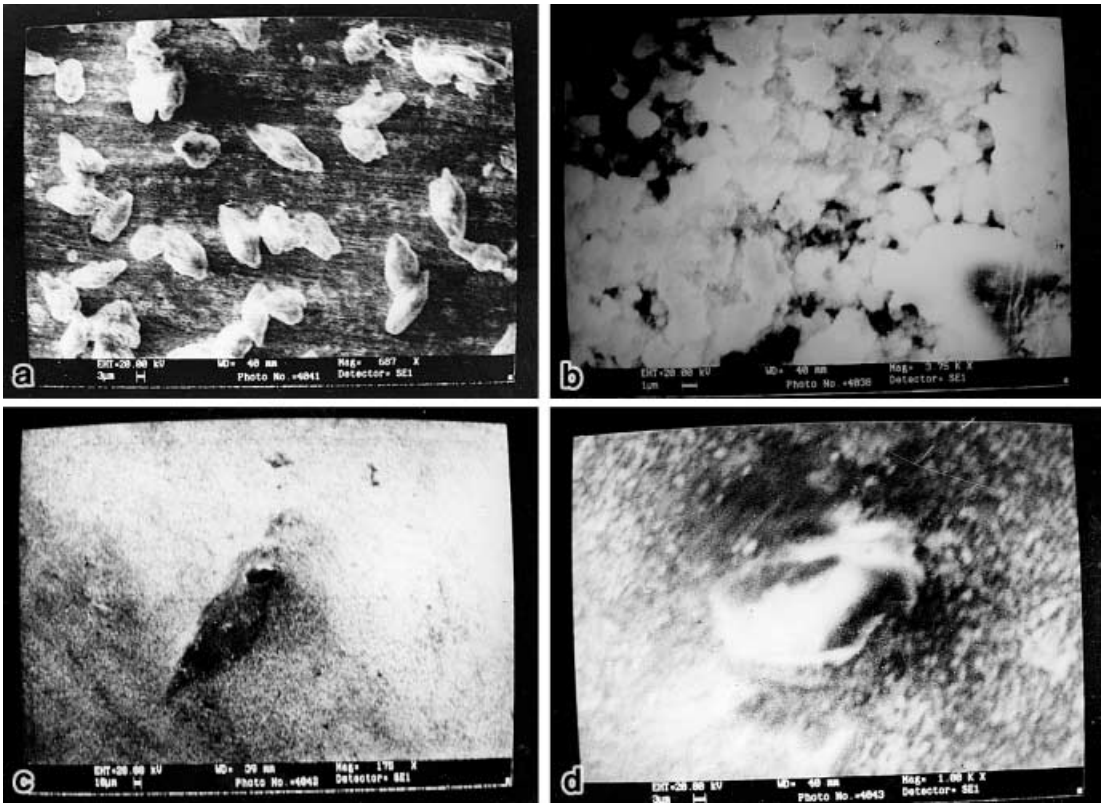

Fig. 9 SEM images of Cu in TEA.3HF after an anodic sweep at 1 mV s^{-1} between 0.7 and 1.2 V: **a** ×687, **b** ×3750; SEM images of Cu after one anodic/cathodic sweep in the same potential range: **c** ×175, **d** ×1000

in TEA.3HF leads to significant enhancement of the anodic dissolution peak, especially in the a_2 potential region (Fig. 10a). The voltammogram shows only slight variation even when twice the amount of water was used under identical conditions (Fig. 10b). In the presence of water, the anodic peak a_3 becomes much broader, probably owing to the formation of an oxide layer along with the fluoride. The Q_c/Q_a values decrease substantially with increasing additive content and even go below 50% (Table 4). All these data suggest substantial solubility of CuF_2 in the presence of the additive.

The anodic behaviour of Ag

The anodic behaviour of Ag in TEA.3HF medium is quite similar to that reported earlier by Gatner and Zicha [35]. However, a brief discussion of the results for comparative purposes is made here. The additive effects and microscopic analysis of the results are also reported for the first time.

Typical multi-sweep cyclic voltammograms of Ag in TEA.3HF at 40 and 80 mV s^{-1} are presented in Fig. 11a and b, respectively. In the first sweep, a small anodic peak around 0.5 V followed by a wave with constant current is noticed. The anodic film growth in this case seems to proceed through AgF film formation (peak region) by direct adsorption, followed by a potential independent-phase growth rate. The AgF phase growth pattern, for example, is similar to the oxide phase growth on Pt group metals through a place exchange mechanism [43]. The anodic oxidation and cathodic reduction peak currents are significantly higher than required for monolayer coverage. The peak currents increase with sweep rate (Table 5). The peak potentials, however, do not vary significantly with sweep rate.

One distinct feature of the anodic behaviour of Ag (which was not discussed in the earlier work) in TEA.3HF medium is the substantially higher Q_c value when compared to Q_a values in the entire potential range investigated. The Q_c/Q_a value is substantially greater than 1, especially during the first voltammetric cycle (Table 5). Chemical conversion of Ag_2O to AgF (similar to that noticed for Cu in the first anodic peak region, see Eq. 1) in the TEA.3HF medium may contribute to a higher concentration of AgF during reduction:

$$Ag_2O + 2TEAF^+.H_2F_3^- \leftrightarrows 2AgF + H_2O + 2TEAH^+.HF_2^- \quad (5)$$

At the slow sweep rate of 40 mV s^{-1}, the dissolution charges exceed 100 mC cm^{-2}. Hence the AgF film formed is also quite thick. The yellow colour of the film could be clearly seen after anodic polarization. The fairly thick fluoride film was also examined through SEM micrographs (Fig. 12a, b); however, the uniform AgF layer contains some pores. After reduction, the Ag

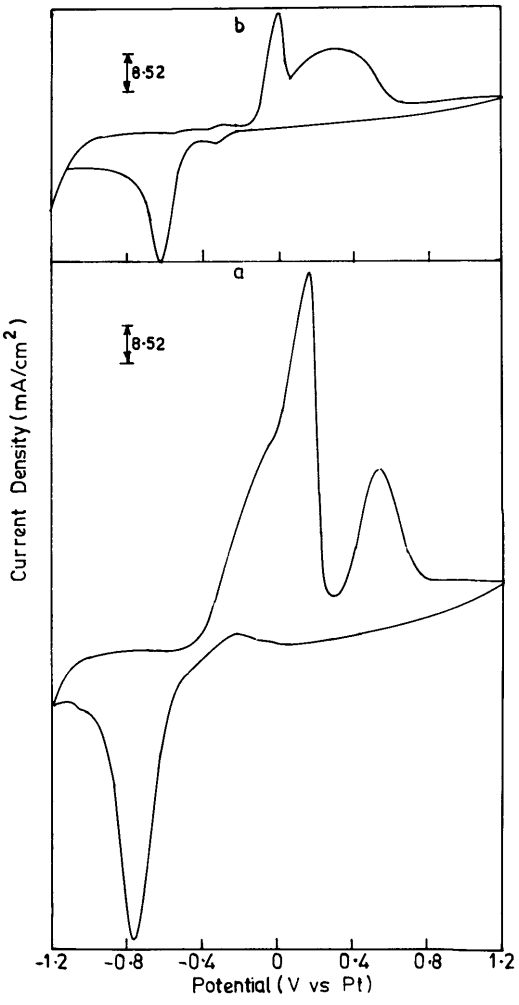

Fig. 10 CVs of Cu in TEA.3HF containing **a** 4% MeCN, **b** 8% water at 160 mV s^{-1}

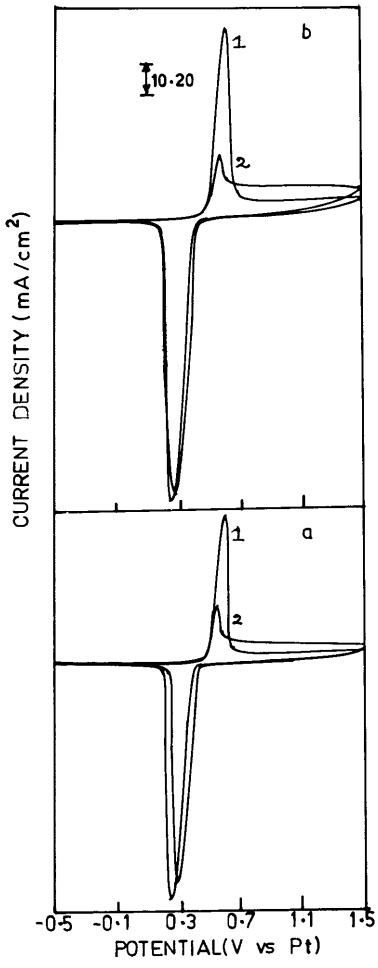

Fig. 11 Multi-sweep CVs of Ag in TEA.3HF at different sweep rates (mV s^{-1}): **a** 40, **b** 80

surface turns black, obviously due to the roughened surface with a higher surface area with finely divided Ag particles. The reduced Ag surface contained large pealed-off surface regions (Fig. 12c) and a higher density of porous regions (Fig. 12d). The rough Ag surface formed during the first anodic and cathodic cycles undergoes much more facile oxidation during the second anodic sweep (Fig. 11a, b). The anodic peak current around 0.5 V increases substantially while the limiting current at higher anodic potential drops substantially. Thus the AgF film growth mechanism itself changes during the anodic sweep.

The Ag/AgF couple is not quite stable to multi-sweep cycling even in the absence of additives. In the presence of additives, further enhancement of anodic dissolution is noticed (Fig. 13). The solubility of AgF in MeCN is significantly higher (Fig. 13a) than that in water

Table 5 Voltammetric features of Ag in TEA.3HF containing various concentrations of MeCN and H_2O at 40 mV s^{-1}

Conc. of MeCN or H_2O (% v/v)	E_{pa1} (V)	E_{pa2} (V)	E_{pc} (V)	i_{pa1} (mA cm^{-2})	i_{pa2} (mA cm^{-2})	i_{pc} (mA cm^{-2})	Q_a (mC cm^{-2})	Q_c (mC cm^{-2})	Q_c/Q_a
0	0.56	–	0.25	16.32	–	79.56	121.8	277.5	2.28
Conc. of MeCN									
1	0.13	–	–0.10	18.36	–	80.58	147.3	260.1	1.77
2	0.26	–	0.18	23.46	–	91.80	235.6	370.3	1.57
4	0.36	0.60	0.18	37.74	12.24	94.86	335.0	472.8	1.41
Conc. of H_2O									
1	0.66	–	0.43	20.20	–	88.74	62.7	248.4	3.96
2	0.68	–	0.33	27.54	–	89.76	112.7	270.8	2.40
4	0.68	0.72	0.20	34.68	15.3	90.78	235.5	546.7	2.34

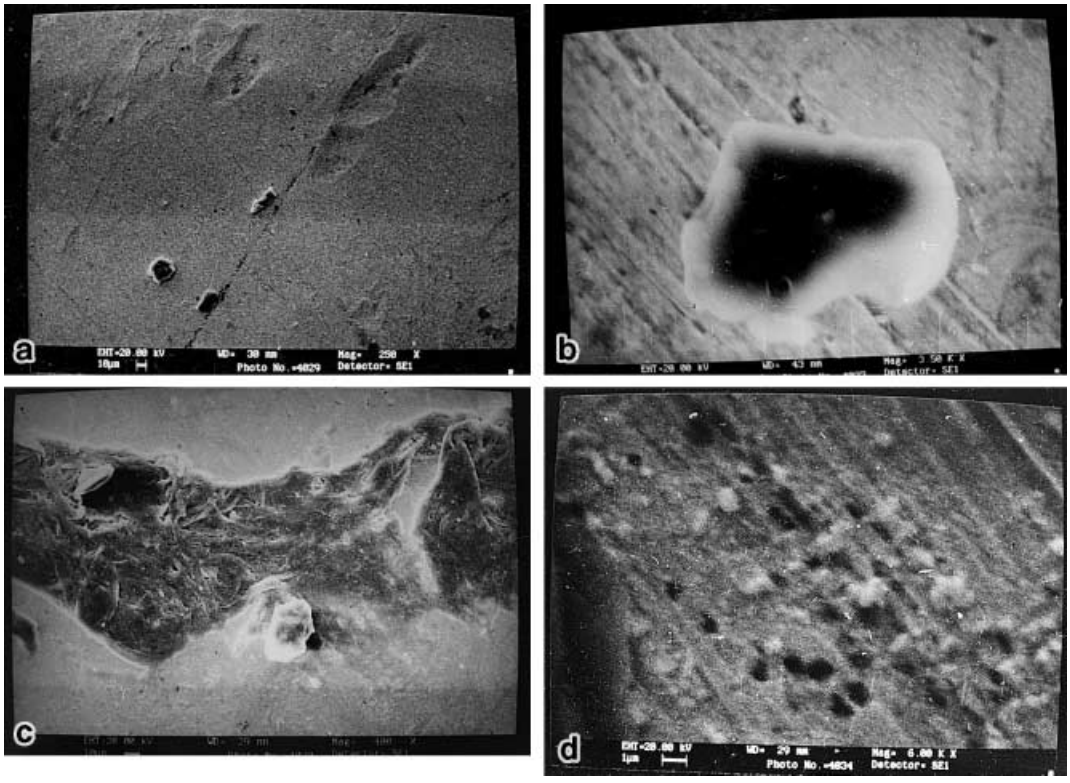

Fig. 12 SEM images of Ag in TEA.3HF after an anodic sweep at 1 mV s^{-1} between 0.0 and 0.7 V: **a** ×250, **b** ×3500; SEM images of Ag after one anodic/cathodic sweep in the same potential range: **c** ×400, **d** ×6000

(Fig. 13b). At such high anodic dissolution levels the substrate becomes very rough during each experiment and establishing reproducible conditions after each experiment becomes a difficult task (Table 5).

Anodic behaviour of Pt and GC electrodes

As pointed out in the Introduction, Pt and GC electrodes have been used as inert electrodes in a variety of fluoride media [4, 12, 31, 32, 33, 34]. In TEA.3HF itself, Pt has been employed as an inert electrode for studying redox reactions [34, 44] as well as organic reactions [37]. A comparative evaluation of Pt, GC and graphite electrodes for fast as well as slow electron-transfer reactions has also been carried out recently [44].

A typical CV of Pt in TEA.3HF at 160 mV s^{-1} (Fig. 14a) shows a small anodic wave around 2 V followed by a significant rise in anodic current around 2.8 V. Similar behaviour was also noticed earlier in liquid HF containing NaF [4]. The higher anodic current around 2.8 V is related to fluorine evolution. Addition of MeCN in small concentrations does not influence the anodic polarization significantly (Fig. 14b). Water also had very little effect. On GC electrodes, significant anodic current was noticed only beyond 2.4 V (Fig. 14c). Fluorine evolution on this electrode occurs only beyond 3.5 V. Addition of MeCN (Fig. 14d) or water once again had very little effect. All these results suggest that these two electrodes can serve as inert electrodes for studying the oxidation of other compounds, even in the presence of trace quantities of water. In contrast to Ni electrodes, Pt and GC electrodes were indeed found to give reproducible voltammetric responses for compounds such as ferrocene, hydroquinone and methyl phenyl sulfide [44].

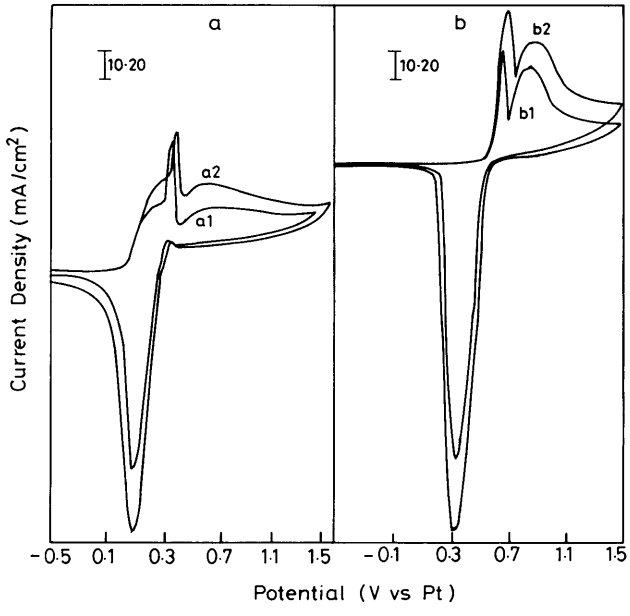

Fig. 13 CVs of Ag in TEA.3HF containing **a** 2% MeCN, **b** 2% H_2O at different sweep rates (mV s^{-1}): **a1**, **b1** 40, **a2**, **b2** 80

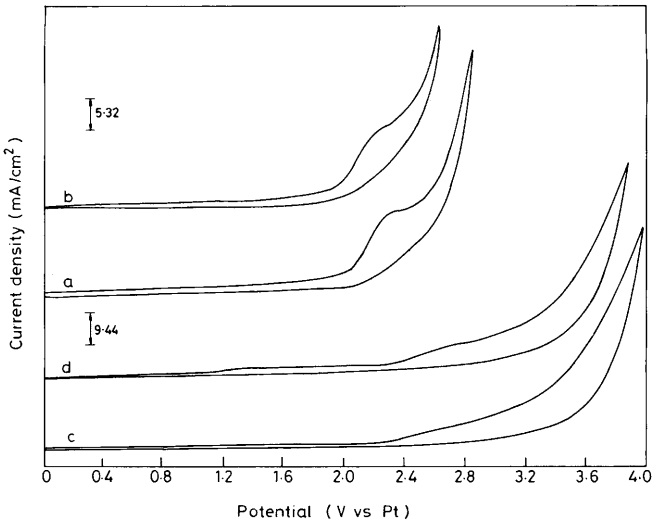

Fig. 14 CVs of **a** GC electrode, **c** Pt electrode in TEA.3HF and **b** GC electrode, **d** Pt electrode in TEA.3HF containing 1% MeCN at 160 mV s^{-1}

Cathodic behaviour of Ni, Cu, Ag, Pt and GCE electrodes

Some experiments were also carried out to evaluate the cathodic behaviour of these electrodes. As long as these electrodes were not polarized in the cathodic potential region corresponding to hydrogen evolution, all these electrodes gave very low cathodic currents until the hydrogen evolution region was reached. A significant hydrogen evolution current was noticed on Pt around –0.5 V. Cu, Ag, Ni and GC electrodes had increasingly higher cathodic limits of –0.55 V, –0.65 V, –0.70 V and –1.0 V, respectively:

$$2TEAH^+ + 2e \rightarrow 2TEA + H_2 \quad (6)$$

Outside this potential range, all the electrodes can be used for studying other solution-phase electro-reduction or metal deposition processes.

Typical CV curves obtained for electro-reduction of 10 mM nitrobenzene in TEA.3HF on all the five electrodes are shown in Fig. 15. No distinct cathodic peak could be observed on Pt electrodes, owing to the hydrogen evolution reaction occurring at lower potentials. Well-defined diffusion-controlled reduction peaks (as evidenced by the measured sweep rate and concentration effects) were observed on the other electrodes. The reduction peak appears like a wave at a slightly more negative potential on the GC electrode. This may be attributed to the general trend of slower electron transfer on carbon electrodes when compared to metal electrodes.

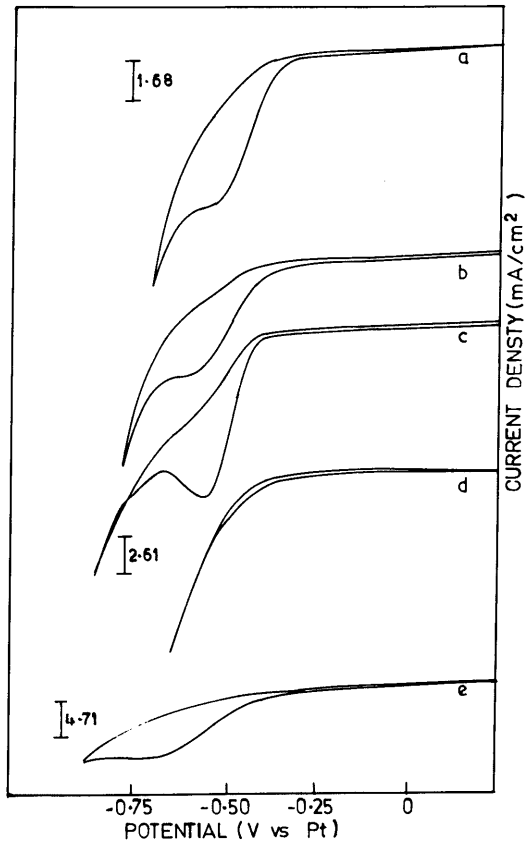

Fig. 15 CVs for the reduction of 10 mM $PhNO_2$ in TEA.3HF on **a** Ni, **b** Cu, **c** Ag, **d** Pt, **e** GC electrodes at 80 mV s^{-1}

Summary and conclusions

The NiF_2 monolayer formation region (< 0.5 V) and bulk NiF_2 nucleative growth region (> 4.0 V) are widely separated for Ni in TEA.3HF medium. In the absence of additives, NiF_2 is highly insoluble and the bulk NiF_2 formed is highly crystalline in nature. Additives, however, induce Ni dissolution in the monolayer formation region as well as in the bulk film growth region. While acetonitrile enhances dissolution of Ni, water induces Ni dissolution as well as hydrolysis of NiF_2, leading to the formation of oxides and oxyfluorides. The NiF_2 film formed is not reducible during cathodic polarization.

During anodic polarization of Cu, CuF_2 monolayer formation occurs very close to the bulk phase growth region, which is controlled by a dissolution-precipitation mechanism. At more positive potentials, another direct film-growth process involving trapped HF molecules is noticed. The CuF_2 formed in all the three anodic potential regions is reduced at the same cathodic peak potential region. The Cu/CuF_2 redox couple can be cycled many times without significant loss of the film. Cu is thus a suitable reference electrode material for this medium. The Ag/AgF couple, however, is not quite stable in this medium. The AgF growth mechanism itself changes with potential cycling. During anodic/cathodic cycling, the roughness of silver electrode changes significantly. For both Cu and Ag electrodes, MeCN enhances the anodic dissolution more effectively than water. Water also enhances the hydrolysis of salts and passivation to some extent.

In TEA.3HF medium, Pt and GC electrodes function as ideal polarizable electrodes in the anodic potential region. The background currents on these electrodes are quite high. The electrode process responsible for high background currents on Pt and GC electrodes deserve further investigation. Pt and GC electrodes show good anodic voltammetric responses for all organic species. In the cathodic potential region, however, all five electrodes can be used as inert electrodes, limited only by their corresponding hydrogen evolution overvoltages. Electroreduction of nitrobenzene, for example, could be observed on all the electrodes except Pt owing to its low hydrogen overvoltage.

Acknowledgements The authors thank the Director, CECRI, Karaikudi, for his keen encouragement during this work. The authors thank Volkswagen, Stiftung, Germany, for financial support. V.S. thanks the CSIR, New Delhi, for the award of fellowships.

References

1. Hackerman N, Snavely ES, Fiel LD (1967) Corros Sci 7:39
2. Hackerman N, Snavely ES, Fiel LD (1967) Electrochim Acta 12:535
3. Childs WV, Christensen L, Klink FW, Koplin CF (1991) In: Lund H, Baizer MM (eds) Organic electrochemistry, 3rd edn. Dekker, New York, p 1103
4. Doughty AG, Fleischmann M, Pletcher D (1974) J Electroanal Chem 51:456
5. Clarke JS, Kuhn AT (1997) J Electroanal Chem 85:299
6. Watanabe N, Haruta M (1980) Electrochim Acta 25:461
7. Zemva B, Lutar K, Chacon L, Fele-Beuermann M, Allman J, Shen C, Bartlett N (1995) J Am Chem Soc 117:1
8. Cauques G, Keita B, Pierre G, Jaccaud M (1979) J Electroanal Chem 100:205
9. Burrows B, Jasinski R (1968) J Electrochem Soc 115:348
10. Doughty AG, Fleischmann M, Pletcher D (1974) J Electroanal Chem 51:329
11. Masson JP, Devynick J, Tremillon B (1974) J Electroanal Chem 54:232
12. Fabre PL, Devynick J, Tremillon B (1980) J Electroanal Chem 113:251
13. Calendra AJ, Ferro CM, Castellano CP (1980) Electrochim Acta 25:201
14. Brown OR, Wilmott MJ (1986) J Electroanal Chem 106:313
15. Gronet H, Devillers D, Vogler M, Hinnen C, Marcus P, Nicolas P (1993) Electrochim Acta 38:2413
16. Gronet H, Devillers D, Duran-Vidal S, Nicholas F, Gunbel M (1999) Electrochim Acta 44:2793
17. Watanabe N, Nakajima T, Tounara H (1998) In: Studies in inorganic chemistry, vol 8. Elsevier, New York, p 1
18. Toja T, Hiralwa J, Chong Y, Watanabe N (1991) Mater Sci Forum 73:609
19. Dumont H, Qian SY, Conway BE (1997) J Appl Electrochem 27:267
20. Rouquette-Sanchez S, Ferry DM, Picard GS (1990) Proc Electrochem Soc, 177th Montreal symposium. Electrochemical Society, Washington, pp 492–513; (1991) Chem Abstr 114:31700
21. Rouquette-Sanchez S, Ferry DM, Picard GS (1989) J Electrochem Soc 136:3299
22. Tasaka A, Ohana Y, Shinaka N, Nishomoto H (1990) Proc Electrochem Soc, 177th Montreal symposium. Electrochemical Society, Washington, pp 481–490; (1991) Chem Abstr 114:31699
23. Tasaka A, Mzuno K, Kamata A, Nishimura K (1991) Mater Sci Forum 73–75:603
24. Tasaka A, Miki K, Ohasui T, Yamaguchi SI, Kanemaru M, Iwanaga N, Aritusuka M (1994) J Electrochem Soc 141:1460
25. Tasaka A, Tsukuda Y, Ohashi T, Yamada S, Matsushita K, Kohmura A, Muramatsu N, Takebayshi H, Mimaki T (1997) Denki Kagaku 65:1086
26. Tasaka A, Tomoo K, Takuwa A, Yamanaka M (1998) J Electrochem Soc 145:1160
27. Tasaka A, Tsukuda Y, Yamada S, Matsuhita K, Kohmura A, Muramatsu N (1999) Electrochim Acta 44:1761
28. Filliandeau DJF, Picard JS (1993) Electrochim Acta 38:1951
29. Huba F, Yeager EB, Olah GA (1979) Electrochim Acta 24: 489
30. Lee SM, Roseman JM, Zartman CB, Morrison EP, Harrison SJ, Stankiewicz CA, Middleton WJ (1996) J Fluorine Chem 77:65
31. Momota K, Morita M, Matsuda Y (1993) Electrochim Acta 38:1123
32. Momota K, Yonezawa T, Hayakawa Y, Kato K, Morita M, Matsuda Y (1995) J Appl Electrochem 25:651
33. Gatner K, Zabinska-Olszak G (1993) Pol J Chem 67:281
34. Gatner K (1993) Pol J Chem 67:1155
35. Gatner K, Zicha A (1995) Pol J Chem 69:1315
36. Meurs JHH, Eilenberg W (1991) Tetrahedron 47:705
37. Suryanarayanan V, Noel M (1998) J Fluorine Chem 92:177
38. Chen SQ, Hatakeyama T, Fukuhara T, Hara S, Yoneda N (1997) Electrochim Acta 43:1951
39. Noel M, Chidambaram S (1994) J Electroanal Chem 369:25
40. Noel M, Chidambaram S (1994) J Fluorine Chem 68:121
41. Noel M, Suryanarayanan V, Krishnamoorthy S (1995) J Fluorine Chem 74:241
42. Franz R (1980) J Fluorine Chem 15:423
43. Noel M, Vasu KI (1990) Cyclic voltammetry and frontiers of electrochemistry. Oxford-IBH, New Delhi, p 371
44. Noel M, Suryanarayanan V, Santhanam R (2000) Electroanalysis 12:1039